Rapid chemical and topological ordering in supercooled liquid Cu_{46}Zr_{54}

V. Wessels, A. K. Gangopadhyay, K. K. Sahu, R. W. Hyers, S. M. Canepari, J. R. Rogers, M. J. Kramer, A. I. Goldman, D. Robinson, J. W. Lee, J. R. Morris, and K. F. Kelton

Phys. Rev. B **83**, 094116 — Published 14 March 2011

DOI: 10.1103/PhysRevB.83.094116

Rapid Chemical and Topological Ordering in Supercooled Liquid $Cu_{46}Zr_{54}$

V. Wessels[a,f]*, A.K. Gangopadhyay[a], K.K. Sahu[a,f], R.W. Hyers[b], S.M. Canepari[b], J.R. Rogers[c], M.J. Kramer[d], A.I. Goldman[d], D. Robinson[d,e], J. W. Lee[g], J.R. Morris[g], K.F. Kelton[a]

a) Washington University, Dept. of Physics, St. Louis, Missouri; b) University of Massachusetts, Dept. of Mechanical Engineering, Amherst, MA; c) NASA Marshall Space Flight Center, Huntsville, AL; d) Ames Laboratory, U.S. DOE and Department of Physics and Astronomy, Iowa State University, Ames, IA 50011 e) Argonne National Laboratory, Argonne, IL; f) ETH Zurich, Dept. of Materials, Zurich, Switzerland; g) Oak Ridge National Laboratory, Oak Ridge, TN;

* *Corresponding author email: victor.wessels@mat.ethz.ch*

ABSTRACT

Evidence for rapid ordering in a supercooled $Cu_{46}Zr_{54}$ liquid, obtained from high energy x-ray diffraction in a containerless processing environment, is presented. Relatively sudden changes were observed in the topological and chemical short-range order near 850°C, a temperature that is 75°C below the liquidus temperature and 465°C above the glass transition temperature. A peak in the specific heat was observed with supercooling, with an onset near 850°C (the same temperature as the onset of ordering) and a maximum near 700°C, consistent with the prediction of a molecular dynamics calculation using embedded atom potentials. The chemical and topological ordering measured here are in agreement with predictions of a rapid development of chemically ordered icosahedral clusters in the supercooled liquid.

I. INTRODUCTION

Experimental and theoretical studies suggest that glass-forming ability (GFA) is improved when the local structure (short- and medium-range order) of a supercooled liquid differs significantly from that of the thermodynamically favored, ordered crystalline phases. Such dissimilar order raises the nucleation barrier and decreases the crystal nucleation rates, an hypothesis first proposed by Frank [1]. This connection between liquid ordering and the nucleation barrier was recently confirmed experimentally [2]. Knowledge of the structural evolution in supercooled liquids, particularly on approaching the glass transition temperature,

T_g, is, therefore, important for gaining a deeper understanding of glass formation from the liquid and the thermal stability of the glassy solid. Chemical fluctuations and chemical ordering can also be important for glass formation and stability [3]. However, while chemical ordering has been observed in glasses[4-5], few data exist for supercooled liquids.

To supplement the lack of experimental data, theoretical models of liquid and amorphous structures are often obtained from molecular dynamics (MD) simulations using either *ab initio* methods or empirical pair potentials. However, finite computational resources restrict the size of the ensembles that can be considered in *ab initio* calculations to a few hundred atoms. Further, the slowest quenching rates in MD are still many orders of magnitude faster than those used for experimental studies of liquids or in the fabrication of metallic glasses. Ensembles for MD simulations made with empirical potentials can be larger (several thousand atoms) and slightly slower quenching rates are possible; however, these are still much higher rates than in experimental studies. From experimental data, atomic structures are often obtained using a Reverse Monte Carlo (RMC) approach. The input data are typically the total static structure factors, although in some cases partial structure factors obtained, for example, from neutron diffraction measurements on samples prepared with isotopic substitution, are used. The uniqueness of the RMC method has been questioned, however. Clearly, there are strengths and weaknesses in both MD and RMC methods; therefore, a combination of these approaches, along with experimental data, provides the most complete structural and chemical information.

Due to their relative simplicity, binary liquids and glasses are the best systems for studying changes in local order on approaching T_g. Binary transition metal (TM) bulk metallic glasses (BMGs), however, do not form easily. They have (thus far) been reported in Cu-Zr [6-9], Cu-Hf [10], Ni-Nb [11], and Ni-Ta [12] alloys. The Cu-Zr metallic glasses are particularly interesting since they form BMGs at several specific concentrations over a wide composition range (30 - 60 at.% Zr) [8-9] and have been extensively studied. As mentioned, glass formation may be linked to evolving order in the supercooled liquid state, and it has been suggested that localized bonding and the formation of ordered groups of atoms may enhance glass formation and stability [13-14]. Numerous theoretical studies of Cu-Zr liquids and glasses [15-22] argue for the formation of chemically and topologically ordered clusters in the supercooled liquid, which are also present in the resulting glasses, and which may form networked structures with a high degree of medium-range order [23]. MD studies of the

structural evolution of the liquid, from above the liquidus temperature, T_l, to T_g, for a range of compositions in $Cu_{100-x}Zr_x$ ($35 \leq x \leq 70$) [15-18] and other MG compositions [24], indicate the formation of structural spatial heterogeneities, *i.e.* solute-centered clusters, having a high degree of icosahedral short range order. For the supercooled Cu-Zr liquids examined in those MD studies, a continuous increase in the number of icosahedral clusters was found, with accelerating ordering beginning below T_l, far above T_g. This formation of icosahedral order can introduce topological frustration [25-26] and decrease the atomic mobility [19, 27], improving glass formation, as has been recently demonstrated experimentally [28].

Here we report the results of an experimental investigation of the local structures of several Cu-Zr liquids that were processed in a high vacuum, containerless environment over a wide temperature range using the beamline electrostatic levitation (BESL) technique [29]. Typical behavior was observed in most of the liquids, with the peaks in the total static structure factor and pair correlation function increasing with decreasing temperature, correlated with an increased structural order. In $Cu_{46}Zr_{54}$, however, sudden changes in the local structure and specific heat were observed at a temperature approximately 75°C below the liquidus temperature and 465°C above the glass transition temperature. These results are qualitatively consistent with MD calculations, and indicate rapid chemical and topological ordering in the supercooled liquid.

II. EXPERIMENTAL PROCEDURE

Supercooled $Cu_{100-x}Zr_x$ liquids (x = 36, 54, and 70) were studied using the electrostatic levitation (ESL) technique [29], which combines a containerless, high–vacuum processing environment with real-time high-energy x-ray diffraction measurements. For the levitation experiments of x = 54, small (2-3 mm diameter) spherical samples were prepared from master-alloy ingots made from high purity Cu (99.999%) and Zr (99.97%, primary impurity Hf) by arc-melting on a water-cooled Cu hearth in a chamber that was repeatedly evacuated to ~30 militorr and backfilled with high-purity Ar gas (99.998%). A Ti getter located close to the sample was melted prior to arc-melting to further reduce the oxygen concentration in the chamber. Each ingot was melted two to three times to ensure a homogeneous composition; the duration of each melt cycle was approximately one minute, and mass losses were negligible (0.1% or better). Amorphous ribbons of $Cu_{100-x}Zr_x$ were prepared by crushing the ingots, melting portions by RF-induction heating in a graphite crucible under an Ar atmosphere, and rapidly quenching onto a copper wheel rotating at ~50 m/s. The glass

samples obtained were continuous for 3-10 cm, with an average cross section of 1-2 mm x 20-30 m. A different facility and technique were used to prepare the samples with x = 36 and 70 than that used for the sample with x = 54; for x = 36 and 70, master-alloy ingots were instead prepared using crystal bar Zr (99.97% purity) and injection casting into a 1.5mm Cu-mold.

For the structural studies of the levitated liquids, the electrostatic levitation facility from NASA Marshall Space Flight Center was incorporated into the 6ID-D beamline of the Advanced Photon Source, Argonne National Laboratory. The spherical samples were levitated inside the BESL chamber under high vacuum (~10^{-7} torr) and heated to 100-300^{o}C above the liquidus temperature using a high-power diode laser. High-energy x-rays (129 keV, 0.0958(6) Å) were used in a transmission geometry to provide a scattering range of $0.8 \leq q \leq 14$ Å^{-1}, limited at low-q by a tungsten beam-stop that protected the detector from the transmitted beam, and at high-q by the size of the Be exit window (technical details can be found in [29]). A collimator was placed inside the chamber immediately after the Be entrance window, to eliminate scattering of the primary x-ray beam from the window and air-scattering before the window. The beam-stop was placed just outside the exit window to again minimize window- and air-scattering of the transmitted x-ray beam. The sample-to-detector distance and its orientation relative to the beam normal were determined using a levitated silicon sphere. For the BESL measurements, diffraction patterns were obtained using a GE Revolution 41-RT detector (details of its application in high energy XRD can be found elsewhere [30]). Room temperature diffraction data for the as-quenched metallic glasses were separately obtained in transmission geometry using 100 keV x-rays and a MAR345 area detector.

The measured scattering intensities were corrected to remove the background of the chamber and air, and analyzed using the PDFgetX2 software [31], correcting for incoherent (Compton) and multiple scattering, to obtain the total static structure factor, $S(q)$, and total pair distribution function, $g(r)$, for all of the liquids that were studied. Liquid atomic structures at each temperature were obtained from these data using the Reverse Monte Carlo (RMC) method [32]. The local order in these structures was characterized using the Honeycutt-Anderson (HA) index method [33].

The liquid specific heat was determined as a function of temperature from the measured temperature-time curves during free radiative cooling using the Stefan-Boltzmann equation,

$$mC_{\mathrm{p}}\frac{\mathrm{d}T}{\mathrm{d}t}=-\sigma_{\mathrm{B}}A\varepsilon_T\left(T^4-T_{\mathrm{o}}^4\right),$$

where m, C_p, $\mathrm{d}T/\mathrm{d}t$, σ_{B}, A and ε_T, are the sample mass, specific heat, cooling rate, Stefan-Boltzmann constant, sample surface area, and hemispherical emissivity, respectively. The emissivity was determined by matching the measured temperature to the known value at the liquidus. Since the temperature dependence of the emissivity is unknown, but is generally small for metallic liquids, it was assumed to be constant (for the Cu-Zr liquids $\varepsilon_T = 0.2$ was used). The temperature-dependent liquid density was determined from the mass and volume, estimated from the image analysis of the liquid droplets using a photographic edge-fitting technique described elsewhere [34].

III. RESULTS AND DISCUSSION

Figure 1 shows representative temperature/time curves observed during free radiative cooling for the levitated liquids. For liquid $Cu_{64}Zr_{36}$ two stages in solidification were observed (Fig. 1.a). Primary crystallization occurred during recalescence, under nonequilibrium, approximately adiabatic, conditions. In the second stage, solidification continued at the solidus temperature under equilibrium conditions, resulting in a temperature plateau. In contrast, no such plateau was observed during the solidification of $Cu_{46}Zr_{54}$ (Fig. 1.b). In that case, the enthalpy of crystallization was insufficient to raise the temperature of the supercooled liquid to the eutectic melting temperature, indicating that the supercooling was below the hypercooling limit [35].

Figure 2 shows the measured total static structure factor, $S(q)$, and total pair distribution function, $g(r)$, over a range of temperatures for $Cu_{100-x}Zr_x$ liquids for x = 36, 54, and 70. For all compositions studied the peak intensities increase and the widths decrease with decreasing temperature, consistent with ordering of the liquid. A shoulder on the high-q side of the second peak in $S(q)$ appears with supercooling for the $Cu_{64}Zr_{36}$ and $Cu_{46}Zr_{54}$ liquids; this is typically taken to indicate the development of icosahedral short-range order [2, 36]. The peak locations in $g(r)$ move to lower values of r, reflecting an increasing density as the liquid cools and becomes more ordered. A significant difference in the primary (nearest neighbor) peaks of $g(r)$ can be seen when comparing liquids of different chemical composition (Fig. 3). For Cu-rich liquids, the maximum of the asymmetric first peak occurs near 2.75Å, while for Zr-

rich liquids it is near 3.15Å (indicated by the vertical dashed lines in Fig. 3). For the intermediate composition, $Cu_{46}Zr_{54}$, the peak is broader, spanning the range between 2.7 and 3.2Å, due to the overlap of two peaks. The physical meaning of the evolution of these overlapping peaks is described in detail below.

In the as-quenched glasses (dashed curves in Fig. 3) a more pronounced asymmetry, compared to the liquids, can be seen in the first peak of $g(r)$ for all compositions studied. For $Cu_{46}Zr_{54}$ and $Cu_{30}Zr_{70}$ the two local maxima in the glass are at similar locations as the local maxima in the first peak of $g(r)$ in the corresponding liquids. This indicates that the short-range order (SRO) that is already present well above T_g in the highly mobile supercooled liquid is similar to that in the dynamically arrested (quenched) glass. EXAFS data for the $Cu_{46}Zr_{54}$ metallic glass [37] show that the average Cu-Cu, Cu-Zr and Zr-Zr nearest-neighbor separation distances at that composition are 2.54-2.95Å, 2.69-2.95Å, and 3.14Å, respectively, consistent with the results of neutron diffraction studies [38]. It is, therefore, reasonable to attribute the lower-r maximum in the first peak of $g(r)$ in the $Cu_{46}Zr_{54}$ liquid to a combined contribution from Cu-Cu and Cu-Zr pairs, and the one at larger r to only Zr-Zr pairs. It is typically difficult to obtain information on chemical order from x-ray diffraction studies alone; either neutron scattering experiments on alloys with differing isotope substitutions or x-ray scattering studies near the absorption edges of the elements are generally required. However, in the case of the $Cu_{46}Zr_{54}$ liquid, the clear separation and the nearly equal weighting of the partial $g(r)$s make it possible to infer that information directly from changes in the total $g(r)$.

The evolving chemical order can be seen by examining the difference between $g(r)$ measured at various temperatures during isothermal holds at decreasing temperature and $g(r)$ measured at 1100°C (above the liquidus temperature), i.e. $\Delta g(r) = g_t(r)-g_{1100°C}(r)$, shown in Fig. 4.a. From that figure it can be seen that the two local maxima have nearly equal intensity for temperatures 900°C and above, while for temperatures 800°C and below the intensity of the local maxima at lower r increases faster than the one at higher r, and becomes dominant. Based on the assignments of the two local maxima to different atomic pairs, as described earlier, the temperature dependence of the total $g(r)$ indicates a more rapid rise in the contribution from pairs containing Cu atoms. Such an increasing preference for certain atomic pairs as nearest neighbors signals a rapid development of chemical SRO in the supercooled liquid below 850°C. These data were obtained for isothermal holds; the same

rapid development of chemical SRO was observed at the same onset temperature (850°C) during free radiative cooling (data taken at a nominal 10Hz sampling rate). As will be shown later, this conclusion is also supported by measurements of the specific heat and thermal expansion coefficient.

To quantify further the evolution of the chemical order with changing temperature, the ratio of the magnitudes of the two local maxima in $\Delta g(r)$ was calculated, as shown in Fig. 4.b. The ratio is essentially constant at high temperatures but rapidly increases as the temperature is lowered below approximately 850°C. The evolution of the ratio in Fig. 4.b is reminiscent of the rapid ordering well above the glass transition that was found in the previously-mentioned MD simulations of Cu-Zr liquids during simulated quenching; it further demonstrates that the two well-separated, but overlapping, components (local maxima) of the first peak in $g(r)$, which are clearly observed in the glass, emerge in the supercooled liquid and become more distinct with decreasing temperature on approaching T_g. A similar analysis to that in Fig. 4.b was not possible for the other Cu-Zr liquids, since the individual atomic pair separation distances are not as evenly weighted as in $Cu_{46}Zr_{54}$ and hence produced no distinct local maxima in $g(r)$. Thus, the $Cu_{46}Zr_{54}$ liquid was used for further analysis.

To characterize the topological aspects of this ordering process, atomic configurations were obtained by a RMC fit to the $S(q)$ data and analyzed using the HA index method, as already mentioned. As illustrated in Fig. 5, the agreement between the RMC fit and the data is very good ($3 \leq \chi^2 \leq 7$), capturing the salient features of the low-q peaks, and also fitting well at high q. Figure 6 shows the results of the HA index analysis of the structures obtained from the RMC fit. These results indicate that the configurations are dominated by icosahedral and distorted icosahedral order. For temperatures below approximately 850°C, the icosahedral order (HA index 1551) increases rapidly (33%) and the distorted icosahedral order (HA indices 1431 and 1541) decreases somewhat less rapidly (10%), after initially increasing, indicating an increasing fraction of atoms with more complete icosahedral local symmetry. The amount of crystalline-like order (BCC and HCP/FCC) is smaller and changes smoothly (3%) across the entire temperature range studied. Taken together, the results of the analysis of the measured $g(r)$ (Fig. 4) and the HA index analysis (Fig. 6) suggest a rapid change in both chemical and topological ordering near 850°C. As already mentioned, MD simulation studies by others have shown that icosahedral order develops rapidly in this liquid with decreasing temperature although in, e.g., [16], this evolution is less rapid than in these

experimental data . This could be due to the much faster cooling rates in the MD simulations, which may not adequately simulate the timescale of the observed ordering.

While it is tempting to analyze the chemical SRO in the ensembles obtained from the RMC fits, such detailed information deduced from a RMC fit alone can be misleading unless constraints (such as additional information from EXAFS, partial $g(r)$s or ab-initio MD simulations) are imposed during the fit. However, the RMC method is reliable for determining overall changes in the topological order, due to the high accuracy of the fits to the total $S(q)$.

Additional support for the rapid rise in chemical and topological order comes from measurements of the specific heat ($C_p(T)$), shown in Fig. 7.a for two different cooling cycles of liquid $Cu_{46}Zr_{54}$. The increasing specific heat with decreasing temperature, observed for temperatures from above the liquidus temperature to approximately 750°C, is consistent with the expected behavior for supercooled metallic liquids (e.g. [39]). Interestingly, however, a peak is observed with further cooling below 700°C; the peak cannot be associated with the glass transition, since the temperature of the maximum is approximately 315°C above T_g. It should be noted that the scatter in the data becomes larger in this temperature range, although the existence of a peak appears to be outside of error. The onset of the peak in $C_p(T)$ is near 850°C, the same temperature as the rapid rise in chemical and structural order (Figs. 4a and 6). While the form of the specific heat maximum is reminiscent of a phase transition, the complete set of experimental data does not support that interpretation. The absence of a cooling-rate dependence of the onset of ordering (determined by a comparison between the isothermal and nonisothermal total $g(r)$ data) and the lack of a measurable discontinuous change in density (Figure 8) rule out a first order phase transition. A lack of coincidence of the temperatures of the maximum in the specific heat and the onset of ordering (700°C and 850°C, respectively) rules out a second order transition. The rapid rise in $C_p(T)$, then, likely reflects a continuous ordering process. The observed maximum in $C_p(T)$ corresponds to the temperature where ordering slows down significantly, but is not dynamically arrested as in the glass transition.

Although the density showed a continuous increase with supercooling, the thermal expansion coefficient ($\kappa(T) = -\rho^{-1}\,\mathrm{d}\rho/\mathrm{d}T$), calculated from separate linear fits for both the high (900°C and above) and low (800°C and below) temperature regions, showed a small, but distinct,

change from 6.00×10^{-5} to $6.32 \times 10^{-5} \pm 0.06 \times 10^{-5}$ kg/m^{3}C, respectively. A smaller value for $\kappa(T)$ at higher temperatures is unusual. This is an indication that the nature of the chemical bonding and the anharmonic part of the interaction potential have changed at lower temperatures, consistent with the measured changes in chemical and topological SRO.

The experimental specific heat data are similar to results obtained from MD simulations for a liquid of similar composition, $Cu_{50}Zr_{50}$ using the embedded atom potential developed by Mendelev *et al.* [40]. The calculated specific heat (Fig. 7.b) has a peak with a maximum at a temperature that is close to that observed in the experimental data for $Cu_{46}Zr_{54}$. In agreement with the previous discussion, the enthalpy computed from the MD simulation shows that the ordering is continuous, arising from an evolution of the potential energy landscape. The initially rapid rise in $C_p(T)$ (i.e. the rate of change of the enthalpy with temperature) suggests a rapid decrease in enthalpy due to ordering, followed by a peak, marking a slowing down of the process at lower temperatures. The broader peak in the specific heat for the MD simulations of $Cu_{50}Zr_{50}$, compared with the experimental data for $Cu_{46}Zr_{54}$, likely reflects limitations of the MD simulation due to inaccuracies of the potentials used and the rapid quenching conditions. The MD simulations show very similar results for $C_p(T)$ as the cooling rate is changed from 3.3×10^{13} to 5.0×10^{10} K/s, suggesting that the process underlying the peak in $C_p(T)$ is not strongly dependent on cooling rate.

Similar to the results for the RMC fits to the experimental data for $Cu_{46}Zr_{54}$, the HA indices computed for the atomic configurations generated in the MD simulations for $Cu_{50}Zr_{50}$ show an acceleration in the growth of ICOS and an accompanying decrease in DICOS over the temperature range of the peak in $C_p(T)$ (Fig. 7.b). The similarities between the experimental and MD results support the existence of the experimentally measured peak in $C_p(T)$, for which the data are somewhat limited in the low-temperature regime, and reinforce the conclusion of rapid ordering in supercooled liquid $Cu_{46}Zr_{54}$. That the experimental data change more rapidly indicates that the process may be more cooperative than can be modeled by the fast cooling and small system sizes of the MD simulation.

To understand the possible effect of such ordering in the liquid on crystallization (and similarly glass formation), it is useful to compare the phases that form after recalescence of the supercooled liquid with those predicted by the equilibrium phase diagram of Cu-Zr [41]. Based on a Rietveld refinement of diffraction data, a phase mixture of $Cu_{10}Zr_7$ (orthorhombic,

a = 12.632Å, b = 9.32Å, c = 9.326Å, space group C2ca [42]) and Zr_2Cu (tetragonal, a = 6.456Å, c = 5.279Å, space group I4/mmm) was formed after solidification of the $Cu_{46}Zr_{54}$ liquid (Fig. 9). The same was obtained after devitrification of the as-quenched glass, consistent with other studies [43]. It is interesting that no evidence of the *B2* – ZrCu phase was found during recalescence of the supercooled liquid. By comparing the measured supercooling to the equilibrium phase diagram this can be understood, since the liquid cooled below the phase field of *B2* – ZrCu before solidification. The icosahedral order developing in the liquid likely made it more difficult to nucleate the cubic *B2* phase, enabling the liquid to be more deeply supercooled to a temperature at which the mixture of $Cu_{10}Zr_7$ and Zr_2Cu was stable. Diffraction data during recalescence, taken at a nominal 10Hz sampling rate, indicate that the two phases form essentially simultaneously. It is puzzling, then, that the amount of $Cu_{10}Zr_7$ present in the solidified sample (74 at.%, determined from the Rietveld refinement of Fig. 9) is greater than that predicted from the equilibrium phase diagram (50 at.%, determined using the lever rule). Likely this indicates that the $Cu_{10}Zr_7$ nucleates first and grows rapidly, shifting the composition of the surrounding liquid towards that of the Zr_2Cu phase, allowing that phase to nucleate. From the diffraction data, this must occur rapidly, leading to a cooperative growth of both phases through much of the recalescence.

IV. CONCLUSION

In summary, we have presented and analyzed structural and thermophysical property results for supercooled liquid $Cu_{46}Zr_{54}$, which, taken together, indicate rapid chemical and topological ordering beginning near 850°C, approximately 75°C below the melting temperature (925°C) and 465°C above the glass transition temperature (385°C). The rapid ordering is distinctly different from the gradual ordering typically observed with supercooling in metallic liquids. No evidence for chemical phase separation has been reported in glasses of this composition [43], suggesting that this is not an explanation for the results discussed here. Instead, the data are consistent with a continuous chemical and topological ordering process. While chemical ordering in metallic glasses is not unusual [4-5], to our knowledge this is the first observation of such ordering in a supercooled liquid.

The more rapid growth of the local maximum at lower r, compared to the one at higher r, in the first peak in the total $g(r)$ indicates a change in the local environment of the Cu atoms. The correlation of the RMC results with the results of MD simulations for this composition [16], suggest that this reflects the development of Cu-centered icosahedral clusters, with Cu

and Zr occupying the vertex positions. For temperatures below 850^{o}C these ordered clusters become increasingly favored energetically, as the energy of the system changes rapidly but continuously, with an associated peak in $C_p(T)$. The RMC and MD studies show that the icosahedral order also increases rapidly in the same temperature range, while the distorted icosahedral order decreases, consistent with the development of ordered clusters.

Do the results presented here give possible reasons for glass formation in this alloy? There are many different reasons for glass formation; no single explanation will fit all cases. The observed chemical/topological ordering in $Cu_{46}Zr_{54}$ could play a role. As already mentioned, theoretical studies [16-17, 27] demonstrate that the growth of icosahedral order is responsible for the arrest of liquid dynamics. This decrease in atomic mobility and the increased barrier to the nucleation of crystal phases having a different chemical concentration and containing no short-range icosahedral order would make crystallization more difficult.

It is possible that this ordering and the associated peak in $C_p(T)$ signal the onset of mode-coupling in the liquid. It might also be linked to a fragile-strong transition in the supercooled liquid (which itself could be a manifestation of mode-coupling). A fragile-strong transition has been reported for a multicomponent Zr-based BMG [44], based on direct measurements of the viscosity. To investigate whether this is the case for $Cu_{46}Zr_{54}$, similar experimental measurements of the viscosity above the glass transition temperature (i.e. in the range from 650-1100°C), are needed.

Acknowledgements

The work at Washington University was partially supported by the National Science Foundation under grant numbers DMR-0606065 and DMR-0856199 and by NASA under Contract Nos. NNX07AK27G. and NNX10AU19G. Use of the Advanced Photon Source is supported by the U.S. Department of Energy (DOE), Basic Energy Sciences, Office of Science, under Contract No. DE-AC02-06CH11357.

The work at Ames Laboratory was supported by the U.S. DOE, Office of Science, Basic Energy Sciences under Contract No. DE-AC02-07CH11358.The work of JRM was sponsored by the Laboratory Directed Research and Development Program of Oak Ridge National Laboratory, managed by UT-Battelle, LLC, for the U. S. DOE. JWL's research was performed at the Oak Ridge National Laboratory, Materials Science and Technology Division and sponsored by the Republic of Korea, Ministry of Knowledge Economy, Visiting Scientists Program, under IAN: 16B642601, with the U.S. Department of Energy.

References

1. F. Frank, Proceedings of the Royal Society of London Series A, 1952. **215**(43).
2. K. F. Kelton, G. W. Lee, A. K. Gangopadhyay, R. W. Hyers, T. J. Rathz, J. R. Rogers, M. B. Robinson, and D. S. Robinson, Physical Review Letters, 2003. **90**(19).
3. P. J. Desré, E. Cini, and B. Vinet, Journal of Non-Crystalline Solids, 2001. **288**(1-3): p. 210-217.
4. G. S. Cargill III and F. Spaepen, Journal of Non-Crystalline Solids. **43**(1): p. 91-97.
5. C. N. J. Wagner, Journal of Non-Crystalline Solids, 1985. **76**(1): p. 29-42.
6. D. Wang, Y. Li, B. B. Sun, M. L. Sui, K. Lu, and E. Ma, Applied Physics Letters, 2004. **84**(20): p. 4029-4031.
7. D. Xu, G. Duan, and W. L. Johnson, Physical Review Letters, 2004. **92**(24): p. 245504.
8. D. Xu, B. Lohwongwatana, G. Duan, W. L. Johnson, and C. Garland, Acta Materialia, 2004. **52**(9): p. 2621-2624.
9. Y. Li, Q. Guo, J. A. Kalb, and C. V. Thompson, Science, 2008. **322**(5909): p. 1816-1819.
10. P. Jia and J. Xu, Journal of Materials Research, 2009. **24**(1).
11. L. Xia, W. H. Li, S. S. Fang, B. C. Wei, and Y. D. Dong, Journal of Applied Physics, 2006. **99**(2): p. 026103-3.
12. Y. Wang, Q. Wang, J. Zhao, and C. Dong, Scripta Materialia, 2010. **63**(2): p. 178-180.
13. P. H. Gaskell, Nature, 1978. **276**(5687): p. 484-485.
14. D. B. Miracle, Nature Materials, 2004. **3**(10): p. 697-702.
15. G. Duan, D. Xu, Q. Zhang, G. Zhang, T. Cagin, W. L. Johnson, and W. A. Goddard, Physical Review B, 2005. **71**(22): p. 224208.
16. Y. Q. Cheng, H. W. Sheng, and E. Ma, Physical Review B, 2008. **78**(1): p. 014207.
17. M. I. Mendelev, M. J. Kramer, R. T. Ott, D. J. Sordelet, M. F. Besser, A. Kreyssig, A. I. Goldman, V. Wessels, K. K. Sahu, K. F. Kelton, R. W. Hyers, S. Canepari, and J. R. Rogers, Philosophical Magazine, 2010. **90**(29): p. 3795-3815.
18. G. A. Almyras, C. E. Lekka, N. Mattern, and G. A. Evangelakis, Scripta Materialia, 2010. **62**(1): p. 33-36.
19. N. Jakse and A. Pasturel, Physical Review B (Condensed Matter and Materials Physics), 2008. **78**(21): p. 214204-9.
20. H. L. Peng, M. Z. Li, W. H. Wang, C. Z. Wang, and K. M. Ho, Applied Physics Letters, 2010. **96**(2): p. 021901-3.
21. Y. L. Sun and J. Shen, Journal of Non-Crystalline Solids, 2009. **355**(31-33): p. 1557-1560.
22. L. Yang, J. H. Xia, Q. Wang, C. Dong, L. Y. Chen, X. Ou, J. F. Liu, J. Z. Jiang, K. Klementiev, K. Saksl, H. Franz, J. R. Schneider, and L. Gerward, Applied Physics Letters, 2006. **88**(24): p. 241913-3.
23. M. Li, C. Z. Wang, S. G. Hao, M. J. Kramer, and K. M. Ho, Physical Review B, 2009. **80**(18): p. 184201.
24. H. W. Sheng, W. K. Luo, F. M. Alamgir, J. M. Bai, and E. Ma, Nature, 2006. **439**(7075): p. 419-425.
25. G. Tarjus and et al., Journal of Physics: Condensed Matter, 2005. **17**(50): p. R1143.
26. H. Tanaka, Journal of Physics: Condensed Matter, 2003. **15**(31): p. L491.
27. S. G. Hao, C. Z. Wang, M. J. Kramer, and K. M. Ho, Journal of Applied Physics, 2010. **107**(5): p. 053511-6.
28. Y. T. Shen, T. H. Kim, A. K. Gangopadhyay, and K. F. Kelton, Physical Review Letters, 2009. **102**(5): p. 057801-4.
29. A. K. Gangopadhyay, G. W. Lee, K. F. Kelton, J. R. Rogers, A. I. Goldman, D. S. Robinson, T. J. Rathz, and R. W. Hyers, Review of Scientific Instruments, 2005. **76**(7): p. 073901.
30. J. H. Lee, J. Almer, C. Aydıner, J. Bernier, K. Chapman, P. Chupas, D. Haeffner, K. Kump, P. L. Lee, U. Lienert, A. Micelia, and G. Vera, Nuclear Instruments and Methods in Physics Research A, 2007. **582**(1): p. 182-184.

31. X. Qiu, J. W. Thompson, and S. J. L. Billinge, Journal of Applied Crystallography, 2004. **37**: p. 678.
32. R. L. McGreevy, Journal of Physics: Condensed Matter, 2001. **13**: p. R877-R913.
33. J. D. Honeycutt and H. C. Andersen, Journal of Physical Chemistry, 1987. **91**: p. 4950-4963.
34. R. W. Hyers, Measurement Science and Technology, 2005. **16**: p. 394-401.
35. D. M. Herlach, Materials Science and Engineering: R: Reports, 1994. **12**(4-5): p. 177-272.
36. S. Sachdev and D. R. Nelson, Physical Review Letters, 1984. **53**(20): p. 1947.
37. A. Sadoc, Y. Calvayrac, A. Quivy, M. Harmelin, and A. M. Flank, Journal of Non-Crystalline Solids, 1984. **65**(1): p. 109-129.
38. D. Ma, A. D. Stoica, X. L. Wang, Z. P. Lu, M. Xu, and M. Kramer, Physical Review B, 2009. **80**(1): p. 014202.
39. R. Busch, J. Schroers, and W. H. Wang, MRS Bulletin, 2007. **32**.
40. M. I. Mendelev, D. J. Sordelet, and M. J. Kramer, Journal of Applied Physics, 2007. **102**(4): p. 043501-7.
41. B. Predel, *Cu-Zr (Copper-Zirconium).* in *SpringerMaterials - The Landolt-Börnstein Database*.
42. D. V. Louzguine-Luzgin, A. R. Yavari, G. Vaughan, and A. Inoue, Intermetallics, 2009. **17**(7): p. 477-480.
43. H. R. Wang, Y. F. Ye, Z. Q. Shi, X. Y. Teng, and G. H. Min, Journal of Non-Crystalline Solids, 2002. **311**(1): p. 36-41.
44. C. Way, P. Wadhwa, and R. Busch, Acta Materialia, 2007. **55**(9): p. 2977-2983.

Figure Captions

Figure 1 – The temperature measured as a function of time for $Cu_{(100-x)}Zr_x$ liquids during free cooling for (a) x = 36, (b) x = 54; note the different scales on the time (abscissa) axes, the temperature (ordinate) axes are of the same scale.

Figure 2 – (color online) Total static structure factors (left) and pair distribution functions (right), with changing temperature, for $Cu_{100-x}Zr_x$ liquids with x = 36 (top), 54 (middle), and 70 (bottom).

Figure 3 – The first peak in $g(r)$ for $Cu_{(100-x)}Zr_x$ liquids for (top) x = 36 at 777, 927, and 1127°C, (middle) x = 54 at 650, 900, and 1100°C, and (bottom) x = 70 at 777, 1027, and 1327°C; in all cases the lowest magnitude corresponds to the highest temperature. For each composition, the dashed curve is the $g(r)$ obtained from the rapidly quenched glass. The vertical lines indicate the positions of the partial pair separation distances at room temperature, taken from EXAFS/neutron scattering data [34-35] and MD simulations [36].

Figure 4 – (a) (color online) The differences in the pair distribution functions $\Delta g(r) = g_T(r) - g_{1100°C}(r)$ for $Cu_{46}Zr_{54}$ at T = 1000 (--), 900 (--), 800 (--), 750 (--), 700 (--), and 650°C (--), showing a splitting of the first peak that becomes more distinct as the temperature is reduced. The arrow indicates the increasing magnitude with supercooling. (b) The ratio of the heights of the two distinct components of the first peak in $\Delta g(r)$, with supercooling (error bars are smaller than the symbols), showing a rapid increase near 850°C (1123K).

Figure 5 – (color online) An example of the quality of the RMC fits to the measured $S(q)$ data for supercooled liquid $Cu_{46}Zr_{54}$; the data at 650°C are shown by the solid circles and the fit is indicated by the red line.

Figure 6 – The numbers of HA pairs with various local symmetries for $Cu_{46}Zr_{54}$ liquids as a function of temperature; the ICOS (1551 ●) is the dominant order, and both it and the DICOS (1431▲, 1541▼) show sharp changes near the transition temperature at 850°C (dashed vertical line), while HCP/FCC (1421/1422 ■) and BCC (1661 ►) change more gradually.

Figure 7 – (a) (color online) The specific heat for liquid $Cu_{46}Zr_{54}$ as a function of temperature for two cooling cycles (symbols ● and ■). The scatter between the two data sets reflects the experimental uncertainty; (b) The $C_p(T)$ of a $Cu_{50}Zr_{50}$ liquid and glass calculated from an MD simulation using an embedded atom potential (dash-dot line), and the results of an HA index analysis of the resulting MD configurations (ICOS (1551●) , DICOS (1431▲, 1541▼) , HCP/FCC (1421/1422 ■) and BCC (1661►)).

Figure 8 – The measured density for liquid $Cu_{46}Zr_{54}$; no sudden changes can be seen across the temperature range studied.

Figure 9 – (color online) A Rietveld refinement of the diffraction data for $Cu_{46}Zr_{54}$ after liquid solidification. The fits indicate a mixture of $Cu_{10}Zr_7$ and Zr_2Cu; the input data are shown in red, the predictions from the refined structure in green, and the difference in purple; the reflection positions for $Cu_{10}Zr_7$ and Zr_2Cu are marked with red and black dashes, respectively.

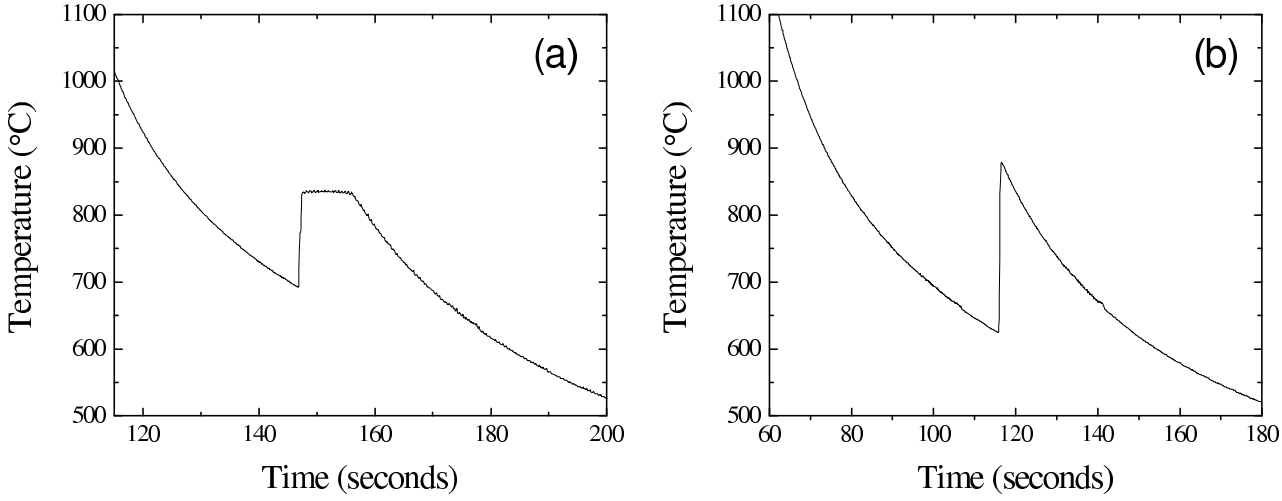

Figure 1 BW11404 20JAN11

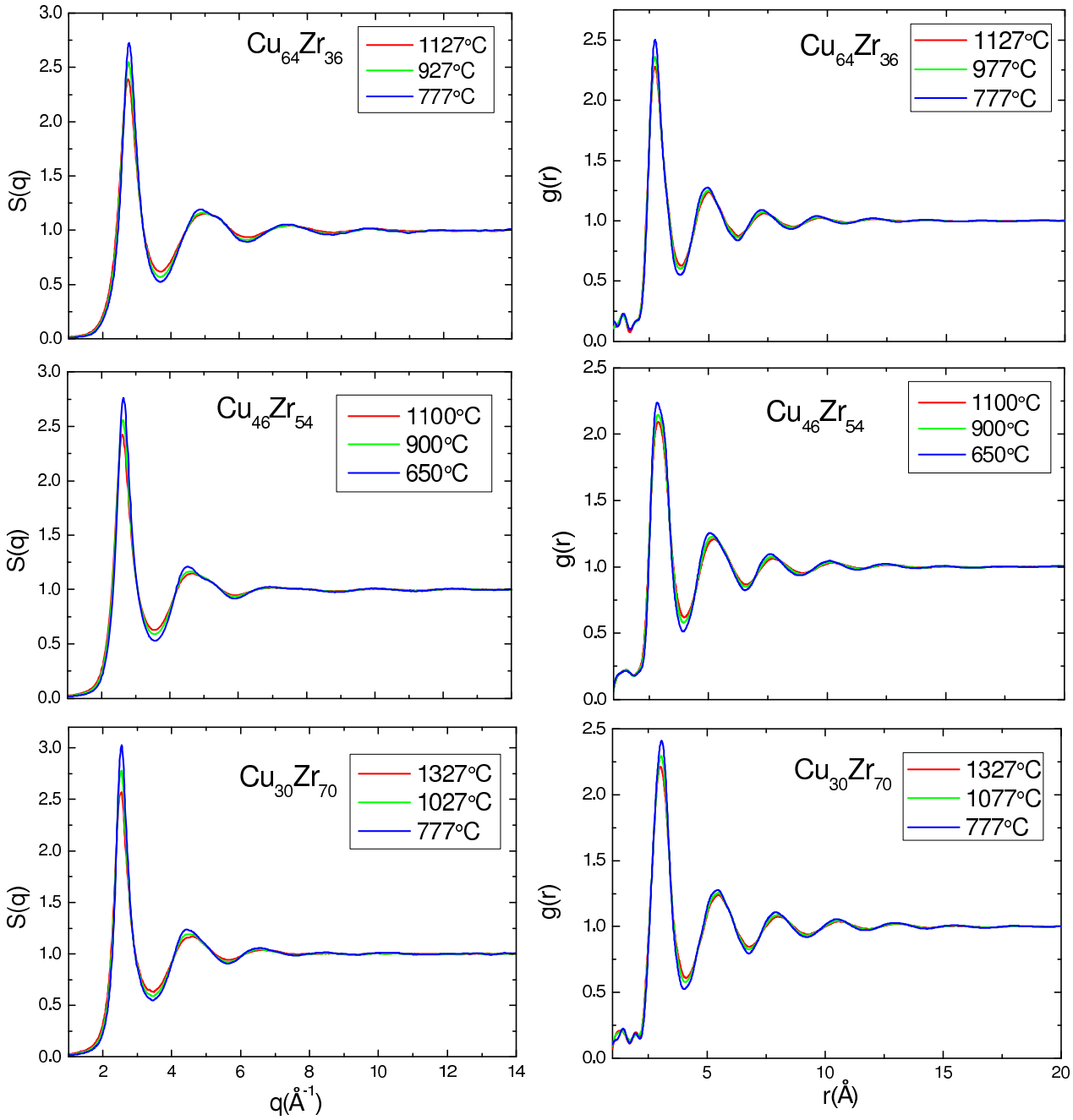

Figure 2 BW11404 20JAN11

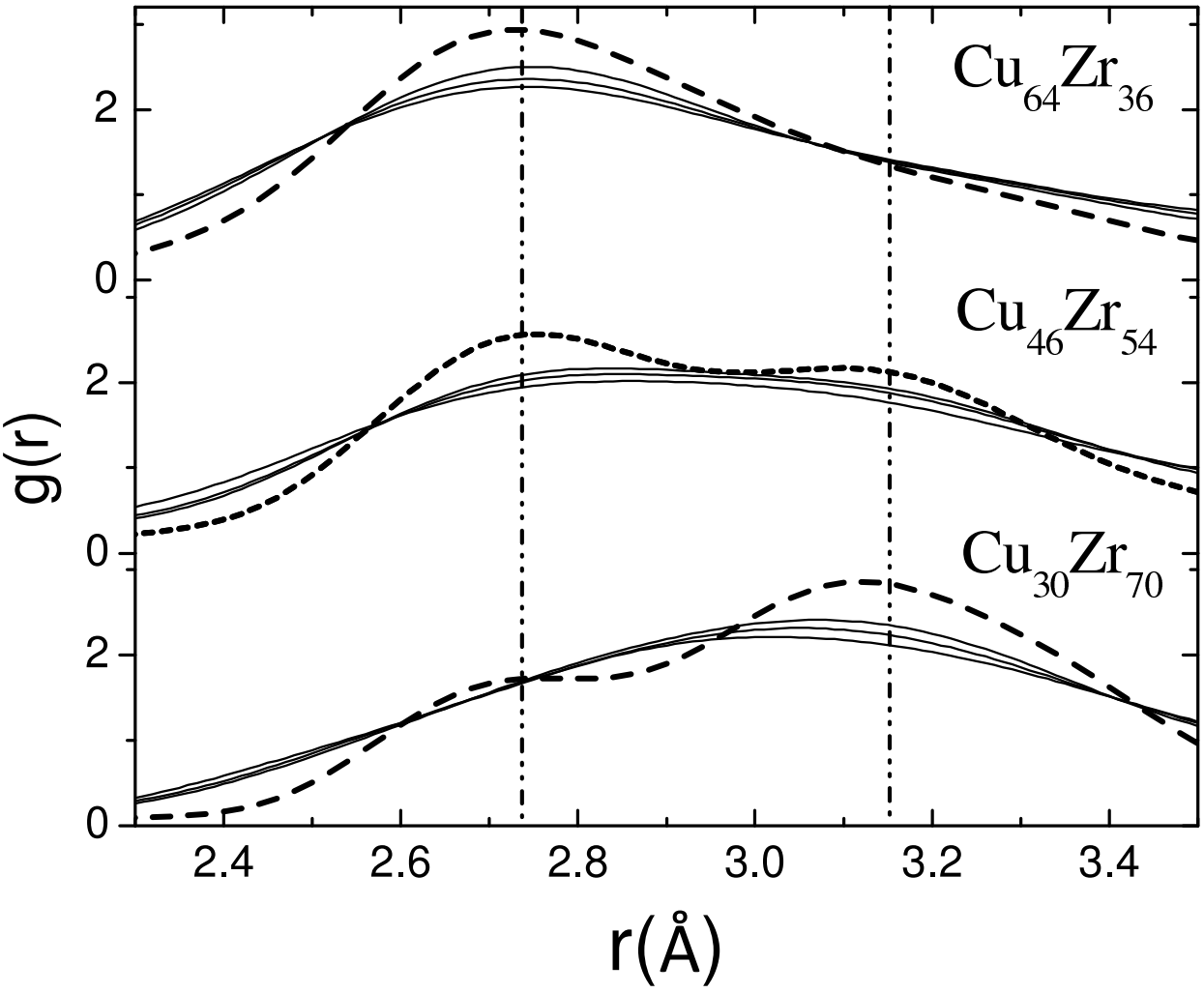

Figure 3 BW11404 20JAN11

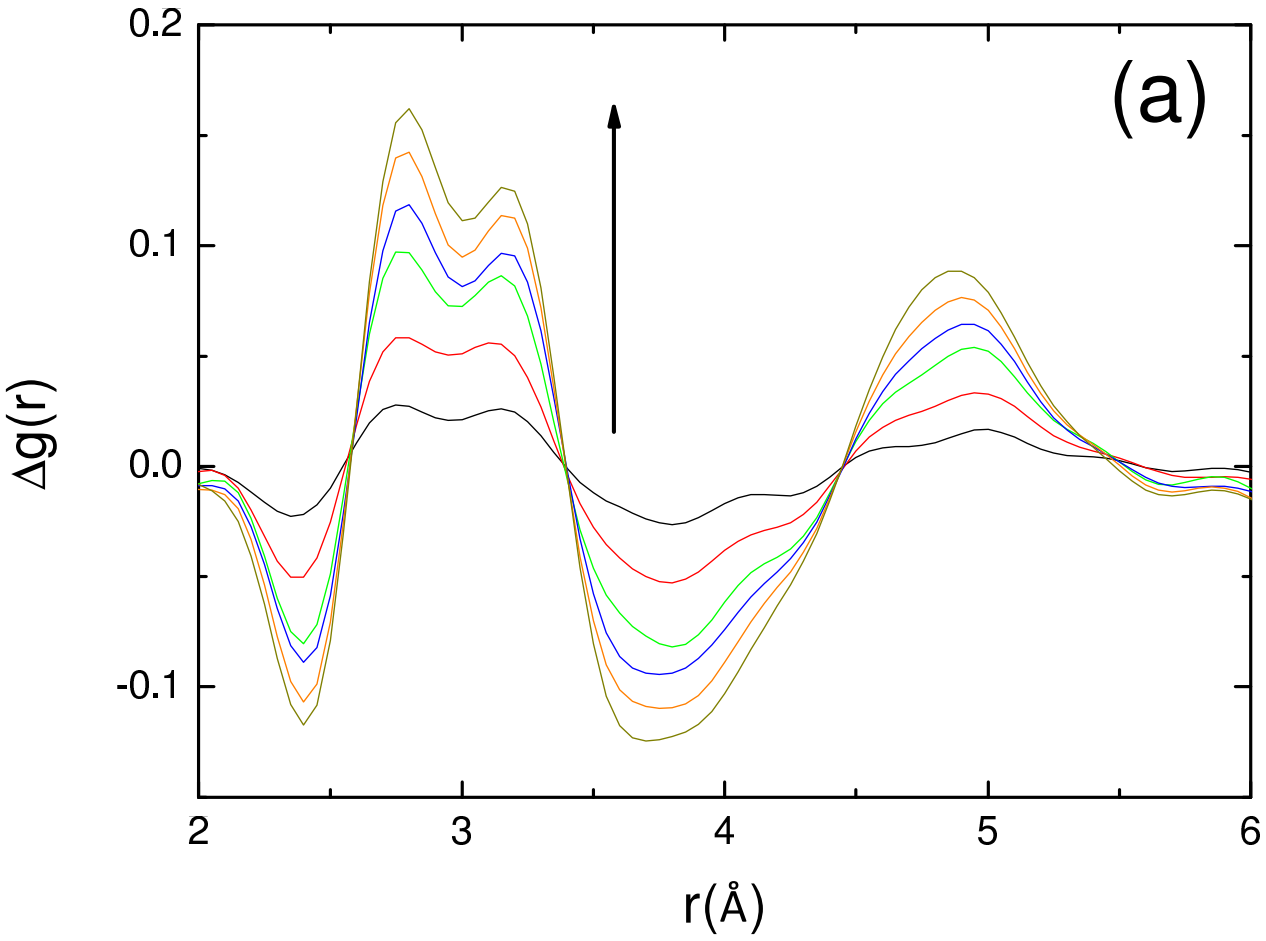

Figure 4a BW11404 20JAN11

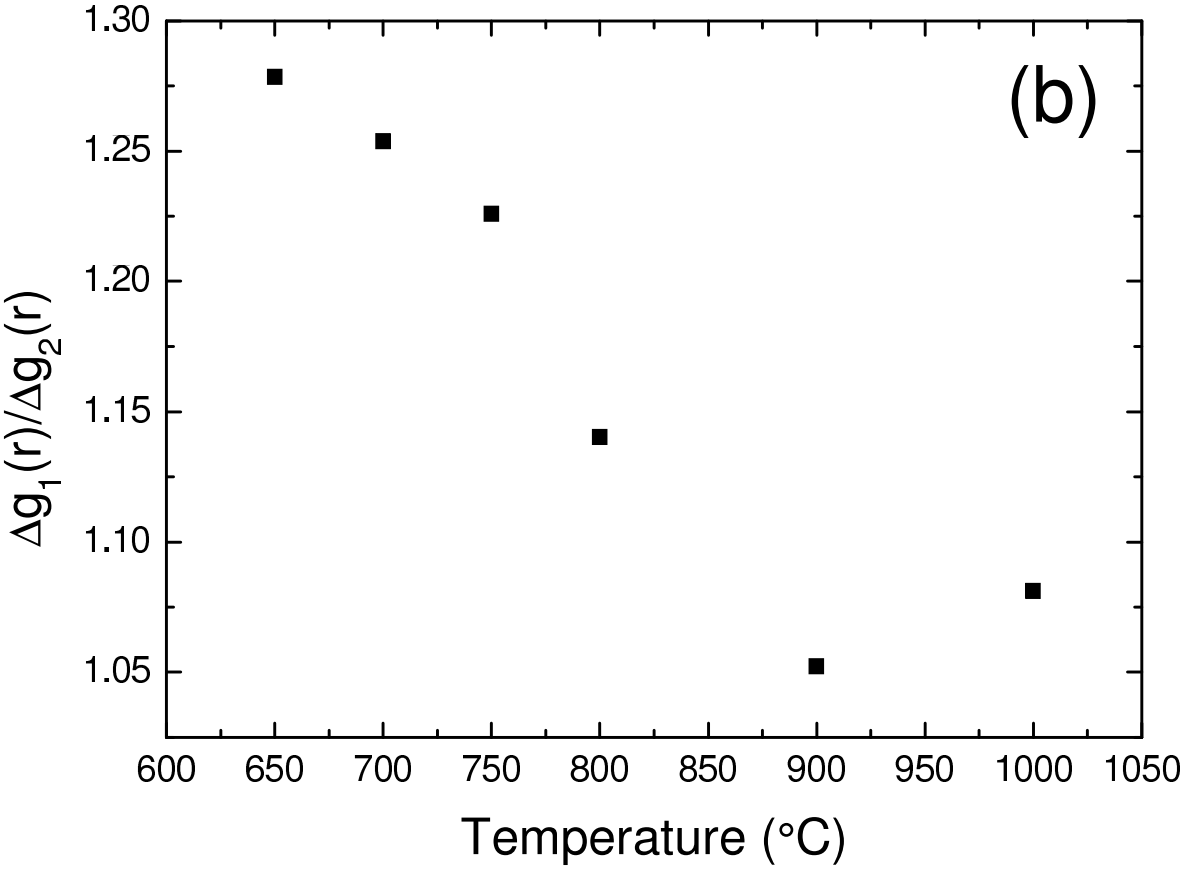

Figure 4b BW11404 20JAN11

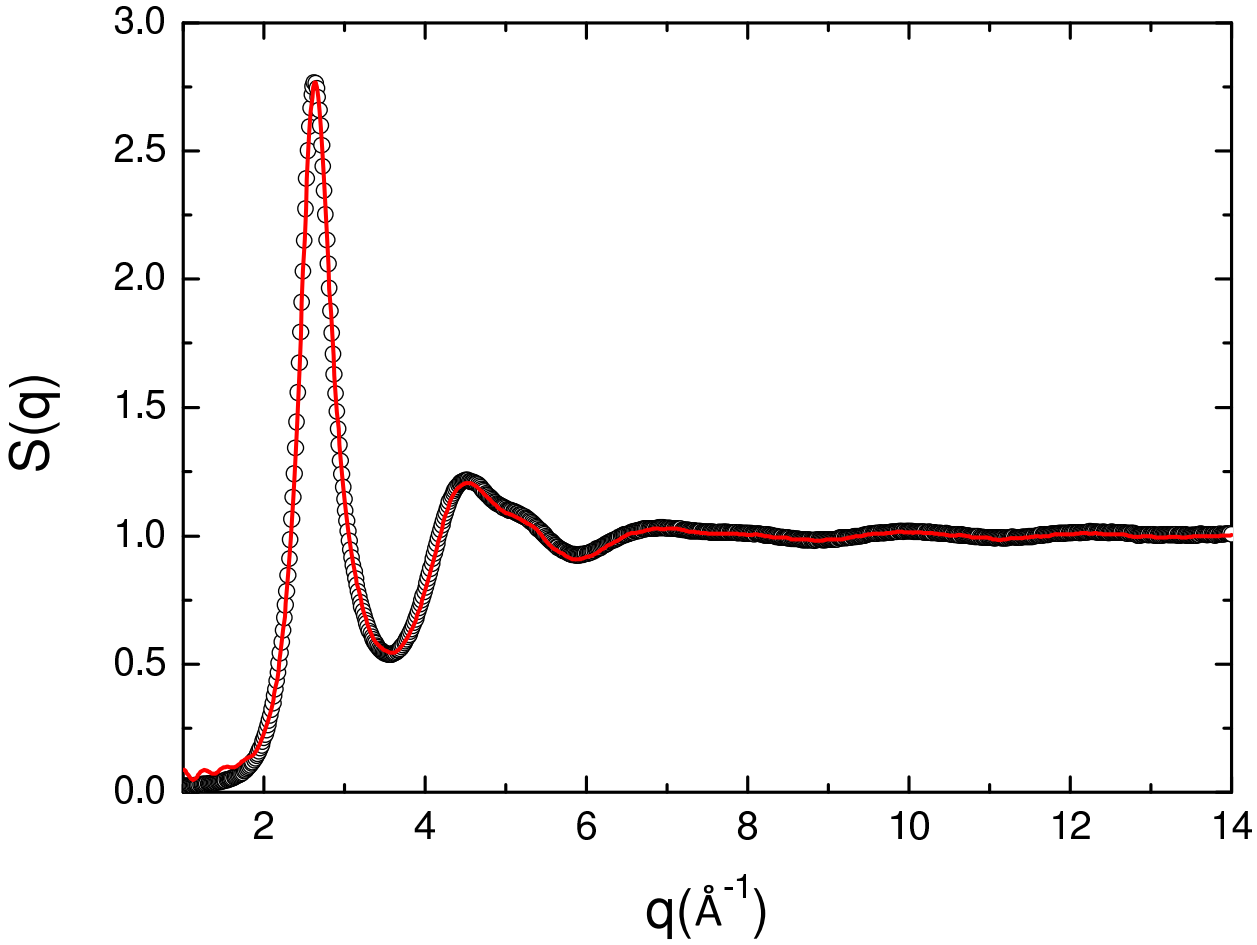

Figure 5 BW11404 20JAN11

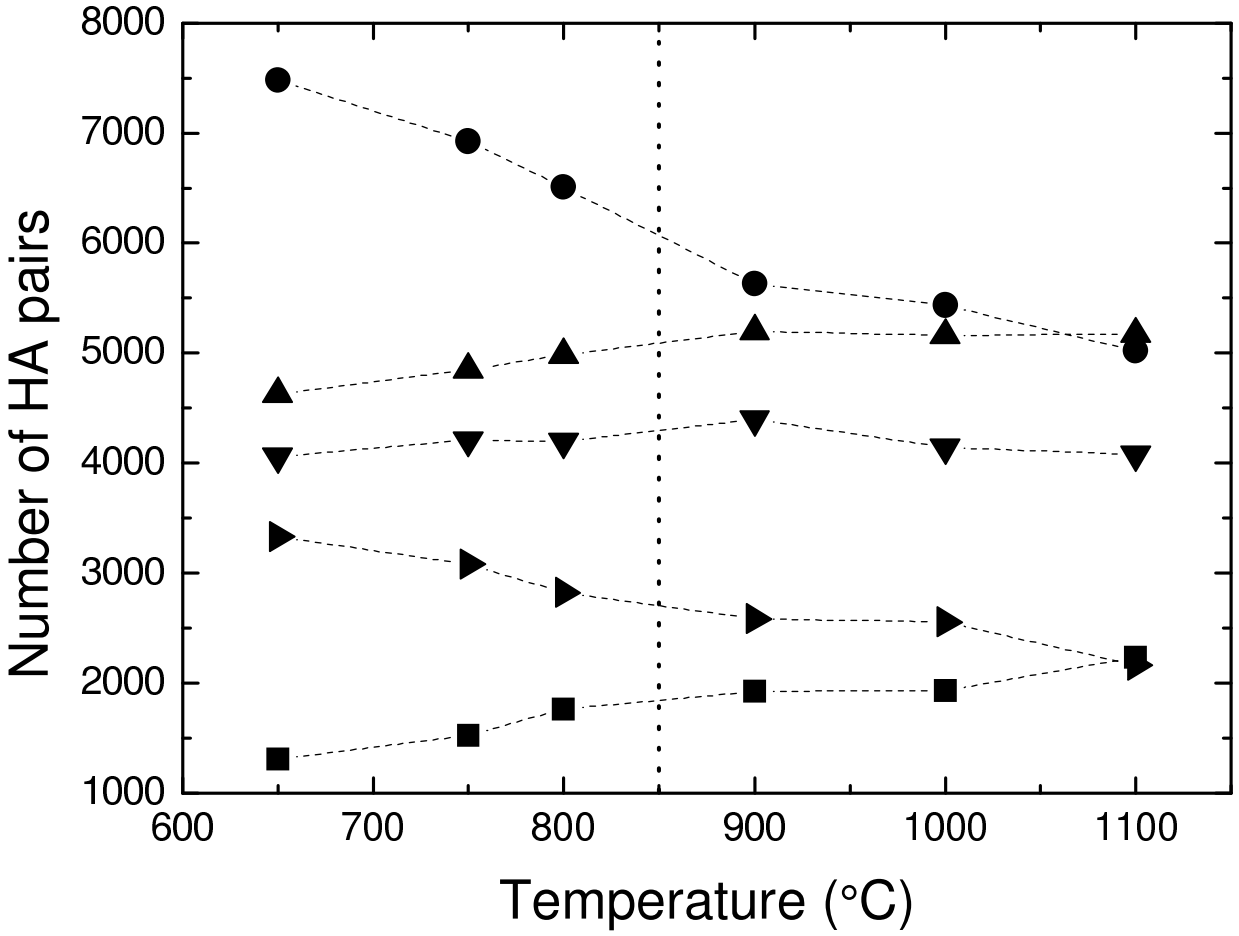

Figure 6 BW11404 20JAN11

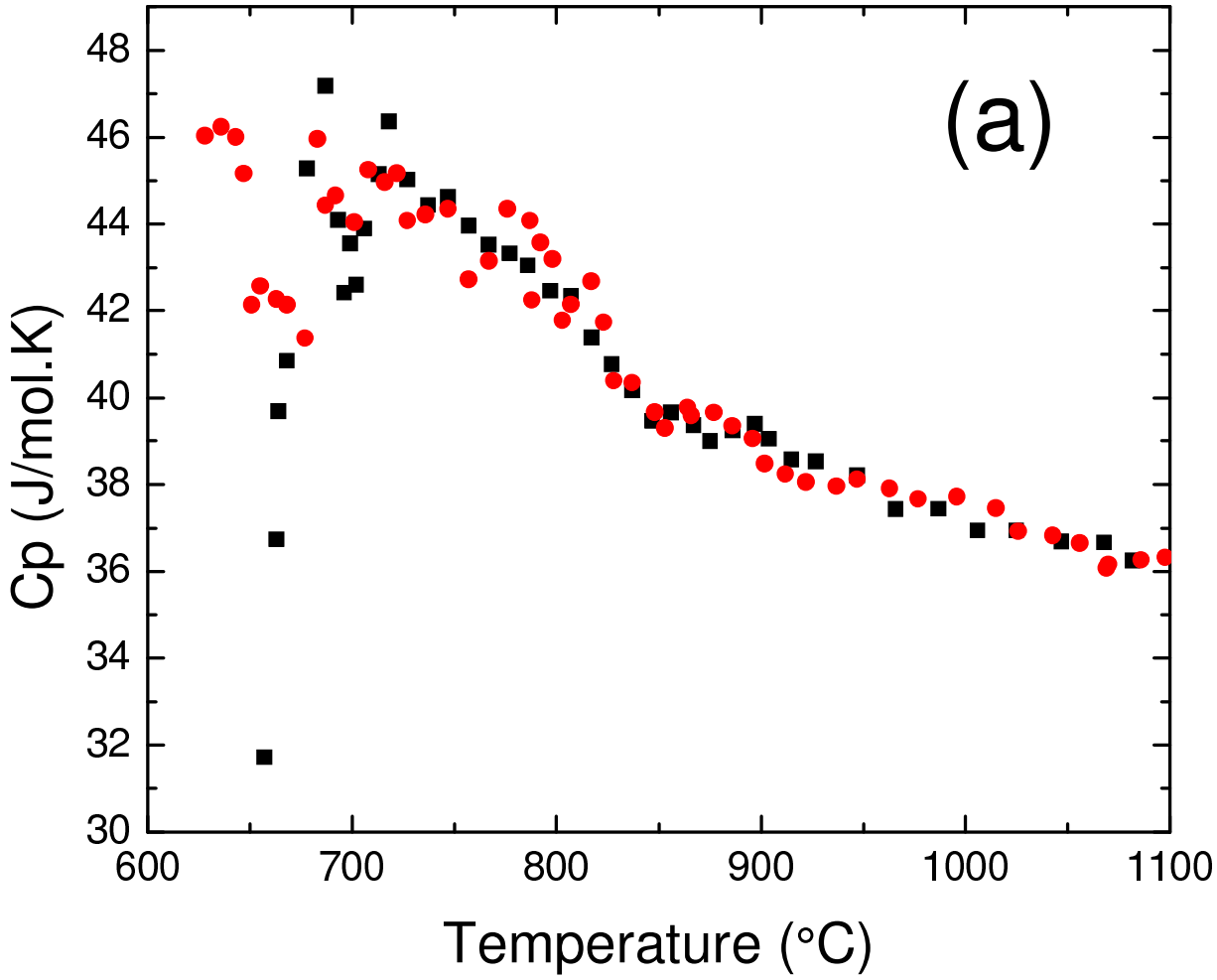

Figure 7a BW11404 20JAN11

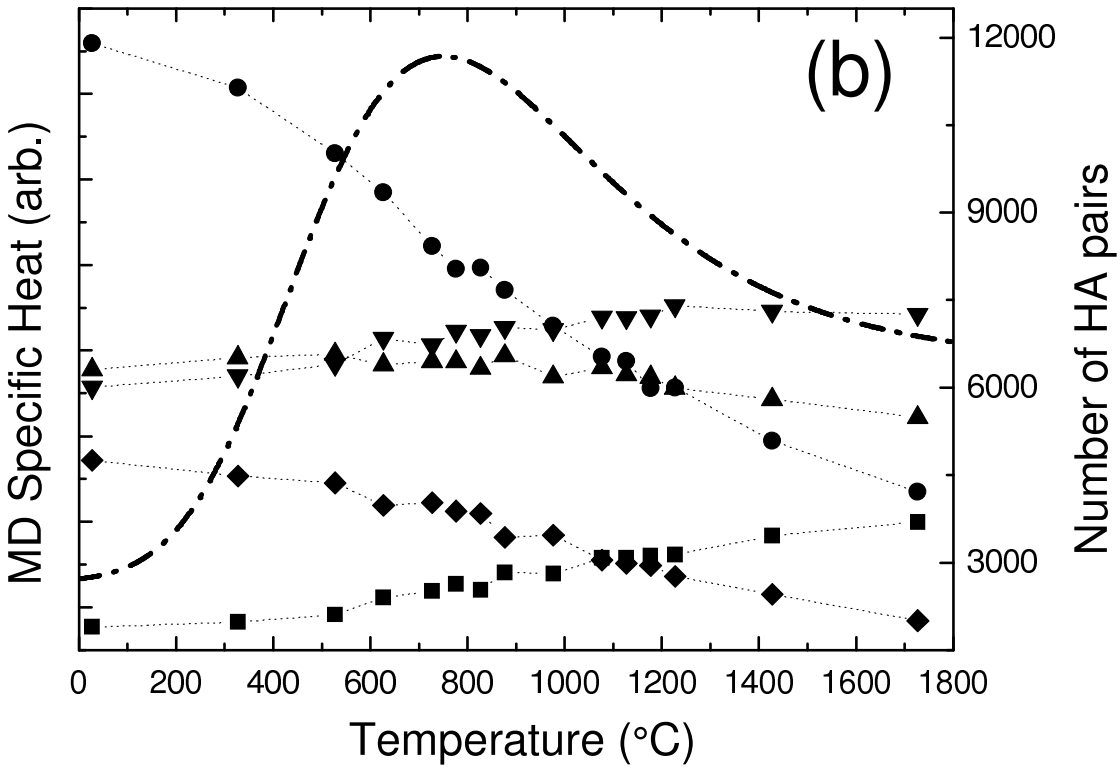

Figure 7b BW11404 20JAN11

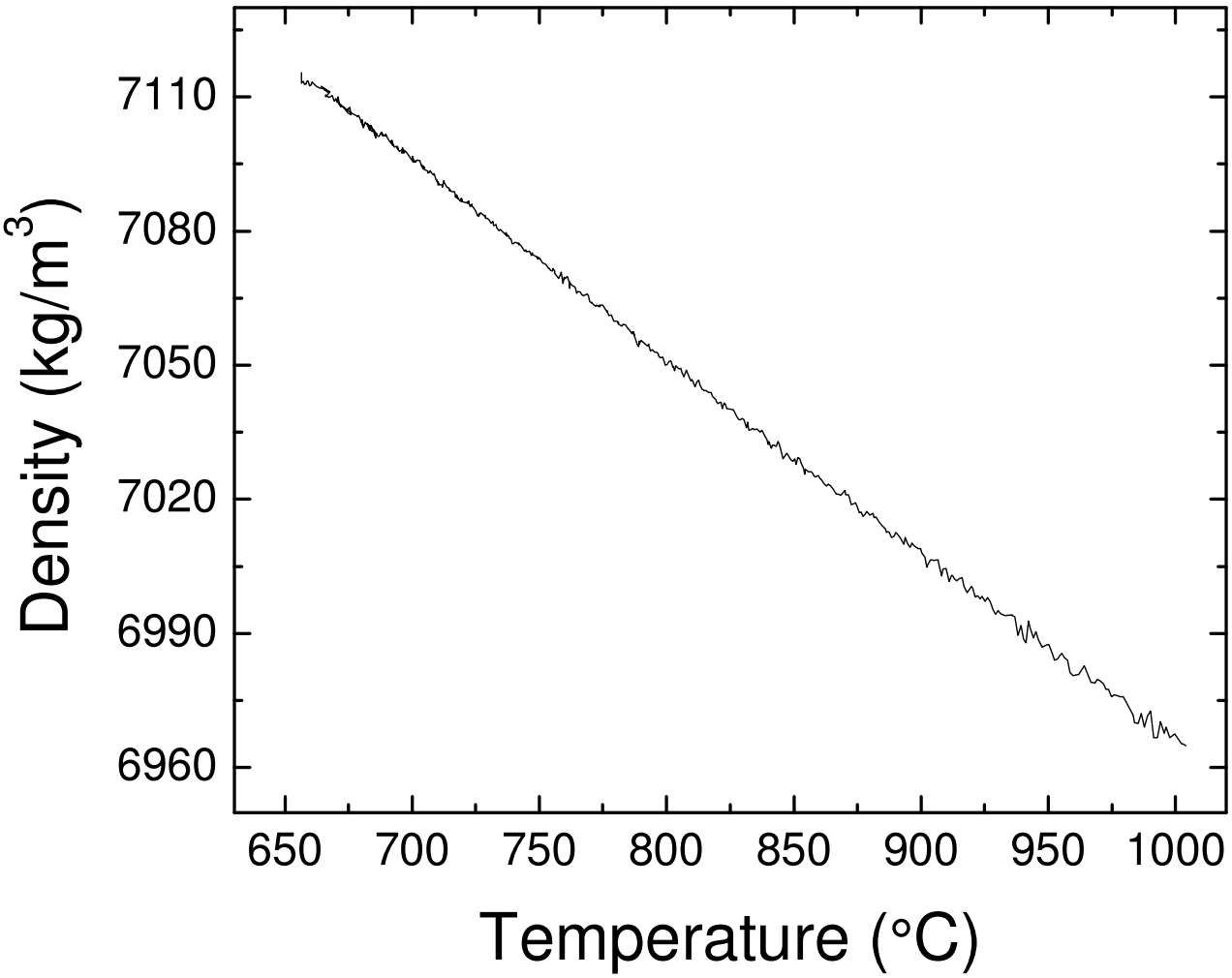

Figure 8 BW11404 20JAN11

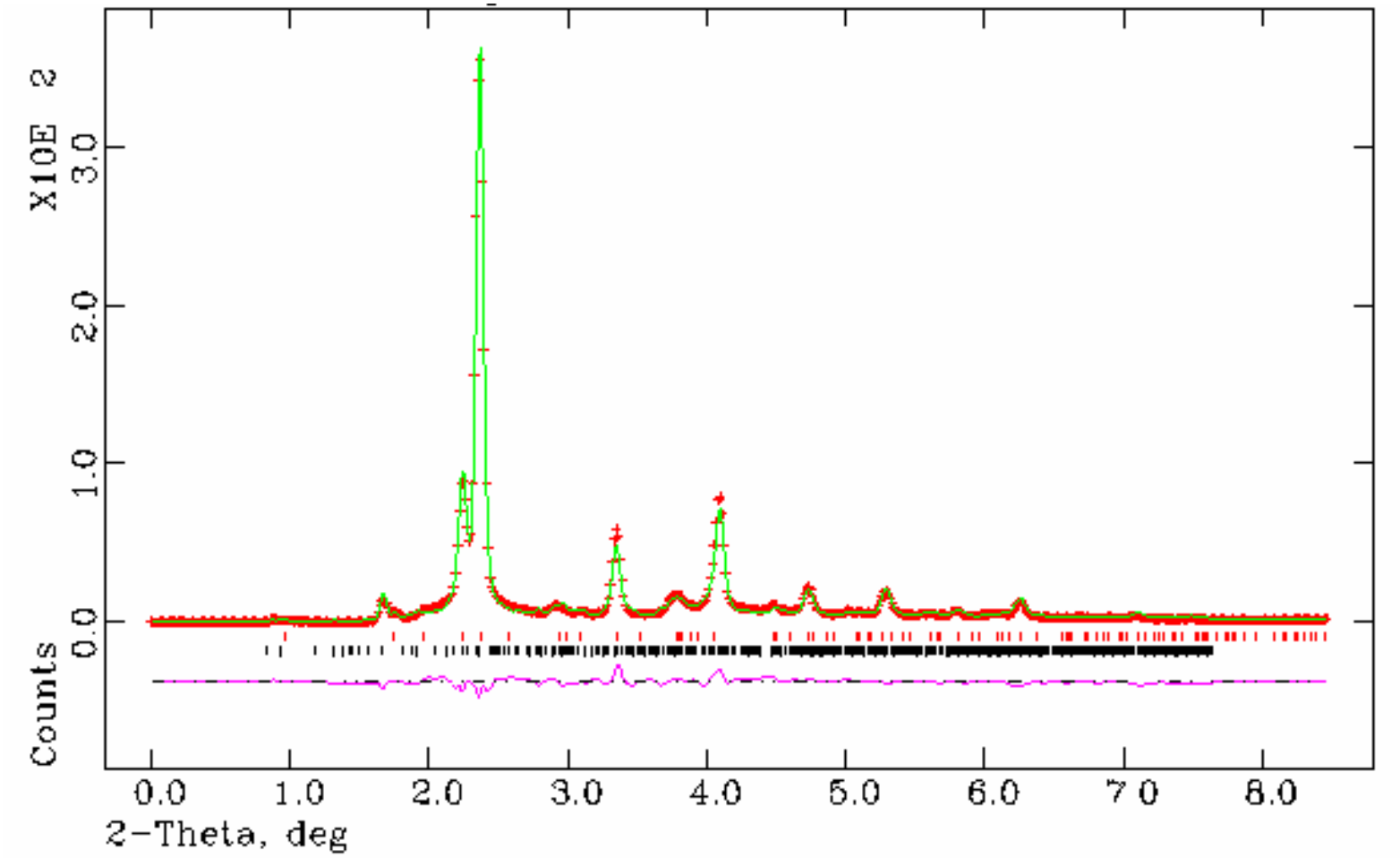
X10E 2
3.0
2.0
1.0
0.0
Counts
0.0
1.0
2.0
3.0
4.0
5.0
6.0
7.0
8.0
2-Theta, deg